Acta Cryst. (1976). A32, 618

Neutron Diffraction Study of Partial Radial Densities in γ-CuCl, Including an Appendix on the Effect of Instrumental Resolution on Radial Density Analysis*

BY J. SCHREURS†

Materials Science and Engineering Department, Northwestern University, Evanston, IL 60201, *U.S.A.*

AND M. H. MUELLER

Materials Science Division, Argonne National Laboratory, Argonne, IL 60439, *U.S.A.*

AND L. H. SCHWARTZ

Materials Science and Engineering Department, Northwestern University, Evanston, IL 60201, *U.S.A.*

(*Received* 11 *August* 1975; *accepted* 4 *February* 1976)

Neutron diffraction has been used to study the structural disorder in γ-CuCl at 25 and 366 °C. Powder patterns of $^{63}Cu^{N}Cl$, $^{N}Cu^{N}Cl$ and $^{65}Cu^{N}Cl$ (N = natural abundance) were treated by integrated intensity (II) and radial density (RD) analyses. Using II, a satisfactory fit to these 366 °C data was made with the anharmonic model described by Sakata, Hoshino & Harada [*Acta Cryst.* (1974). A**30**, 655–661]. This fit resulted in an anharmonic parameter $\beta_{Cu} = 1{\cdot}2 \pm 0{\cdot}6 \times 10^{-12}$ erg Å^{-3}, which is in excellent agreement with the value of $\beta_{Cu} = 1{\cdot}15 \pm 0{\cdot}66 \times 10^{-12}$ erg Å^{-3} obtained from a single-crystal study at room temperature by Sakata *et al.* (1974). To eliminate the indistinguishability of the anharmonic and statistically disordered models inherent in II, an energy analysis was made of the diffuse scattering. It was found that at 25 °C, 50 to 70% of the diffuse scattering is elastic. The non-monotonic κ dependence of this elastic diffuse scattering implies a model of correlated static displacements of Cu atoms and is inconsistent with the anharmonic model. Radial density analyses of the three spectra were fitted to a model based on harmonic vibration to obtain partial radial densities ϱ_{CuCu}, ϱ_{ClCl} and ϱ_{CuCl}. Although the ϱ_{ClCl} was typical of that expected for a solid structure, ϱ_{CuCu} at 366 °C was found to be more 'liquid-like'. Quantitative conclusions from this radial density analysis are limited by the strong dependence of the results on instrumental resolution. An estimate of the effect of instrumental resolution on the measured radial density function is contained in Appendix *B*.

1. Introduction

From the X-ray structural investigations by Miyake, Hoshino & Takenaka (1952), Hoshino (1952, 1954, 1955, 1957) and Miyake & Hoshino (1958) on powder specimens of CuI and CuBr, it appears that the cuprous halides exhibit 'structural disorder' quite similar to that proposed for β-AgI by Helmoholz (1935) and for α-AgI by Strock (1936). Although the zincblende type of structure is accepted for the γ-phases, analysis of integrated intensities invariably yields high values for the cation mean square displacements $\langle u^2 \rangle$ at both room and elevated temperatures.

The expected presence of this 'structural disorder' in CuCl has recently been confirmed by Sakata, Hoshino & Harada (1974), (SHH), who carried out a detailed neutron diffraction study of a single crystal at room and elevated temperatures. SHH have discussed their results in terms of three possible models.

Harmonic model. Vigorous isotropic thermal vibrations of Cu atoms. The atoms in the unit cell of CuCl (zincblende structure of space group $F\bar{4}3m$) have coordinates Cu: 0,0,0; f.c., Cl: $\frac{1}{4},\frac{1}{4},\frac{1}{4}$; f.c. Two isotropic thermal parameters B_{Cu} and B_{Cl} are to be determined.

Anharmonic model. Asymmetric anharmonic thermal vibrations of Cu atoms along the tetrahedral diagonals. In the lowest order of approximation, two isotropic thermal parameters B_{Cu} and B_{Cl} and two anharmonic parameters β_{Cu} and β_{Cl} must be determined.

Disordered model. Statistical disorder of the Cu atom with moderate thermal vibration among the four metastable positions represented by coordinates Cu: $\bar{\delta},\bar{\delta},\bar{\delta}$; $\bar{\delta},\delta,\delta$; $\delta,\bar{\delta},\delta$; $\delta,\delta,\bar{\delta}$; f.c., with δ, B_{Cu} and B_{Cl} to be determined.

SHH noted that for δ small, the anharmonic and disordered models are indistinguishable when analyses of integrated intensities are used. Their fit to 43 independent room-temperature reflections yielded the results displayed in Table 1. Although statistically indistinguishable, SHH favored the anharmonic rather than the disordered model as the former fitted high-temperature data with no adjustable parameters, whereas the latter model could only be made to fit the high-temperature data when a temperature dependent δ was allowed. In the present study, a distinction be-

* Work supported by the U. S. Energy Research and Development Administration.

† This research represents a portion of a thesis submitted by J. Schreurs for the Ph. D. degree in Materials Science and was supported in part by ARPA through the Materials Research Center of Northwestern University. Present address: Westinghouse Corporation, Beulah Road, Pittsburgh, Pennsylvania 15235.

tween the anharmonic and disordered models is made by examination of the diffuse scattering accompanying structural disorder in CuCl.

Table 1. *Results of Sakata et al.* (1974) *for thermal parameters in* CuCl *at room temperature*

Parameters	Harmonic model (R=5·2 %)	Anharmonic model (R=3·7 %)	Disordered model (R=4·0 %)
B_{Cu}(Å^2)	4·4 ± 0·08	4·4 ± 0·08	2·9 ± 0·15
B_{Cl} (Å^2)	2·4 ± 0·04	2·5 ± 0·04	2·3 ± 0·04
β_{Cu} (10^{-12} erg Å^{-3})	–	1·15 ± 0·66	–
β_{Cl} (10^{-12} erg Å^{-3})	–	0·0 ± 1·60	–
δ	–	–	0·024 ± 0·0006

The structural characterization of CuCl has added interest in light of the investigation of liquid CuCl by Page & Mika (1971) (PM). In this study, the partial radial distribution functions for Cu–Cu, Cu–Cl and Cl–Cl distances were determined using the isotopic substitution technique originally suggested by Vineyard (1958) and developed by Keating (1963). PM found that the Cu–Cu distances were virtually uncorrelated at 440 °C (CuCl melts at 430 °C), whereas the Cl–Cl distances show a typical liquid-like behavior with a well defined nearest-neighbor distance followed by rapidly damped oscillations. Since radial distribution analysis is applicable to polycrystalline materials as well as to liquids (Kaplow, 1974), it was thought desirable to repeat the experiment of PM for γ-CuCl as an alternative representation of the disordered solid structure.

2. Theory

The coherent differential scattering cross section (CDSC) for a binary powder at the reciprocal length κ can be written as (see *e.g.* Vineyard, 1958)

$$s(\kappa)=\sum_i \sum_j b_i b_j x_i S_{ij}(\kappa)\,, \tag{1}$$

with

$$S_{ij}(\kappa)=\delta_{ij}+\int_0^\infty 4\pi r[\varrho_{ij}(r)-x_j\varrho_0]\frac{\sin \kappa r}{\kappa}\,\mathrm{d}r\,, \tag{2}$$

and b_i=coherent scattering length of chemical species i, x_i=atomic fraction of chemical species i, $S_{ij}(\kappa)$= partial structure factor for ij scattering, δ_{ij}=Kronecker symbol: $\delta_{ij}=1$ atom if $i=j$, $\delta_{ij}=0$ if $i\neq j$, r=radial distance in a crystal, $\varrho_{ij}(r)$=partial density of ij pairs; the term is the number of j atoms per unit volume to be expected at a distance r from an i atom, ϱ_0=the number of atoms per unit volume to be expected in a random choice of volume element in a crystal.

In the case of neutron diffraction, the b_i are independent of κ and equations (1) and (2) can be readily manipulated into a relation between two functions that form a Fourier sine pair

$$F(\kappa)=\int_0^\infty G(r)\sin \kappa r\mathrm{d}r\,, \tag{3}$$

where F and G are defined as follows:

$$F(\kappa)=\kappa[s(\kappa)-\langle b^2\rangle]/\langle b^2\rangle\,,$$
$$G(r)=\sum_i \sum_j x_i b_i b_j 4\pi r[\varrho_{ij}(r)-x_j\varrho_0]/\langle b^2\rangle\,,$$

where $\langle b^2\rangle=\sum_m x_m b_m^2$, and

$$i,j,m=1,2\,. \tag{4}$$

Since $s(\kappa)$ is observable, $F(\kappa)$ will be referred to as the data function and $G(r)$ as the structure function. Ultimately, one is interested in finding three $\varrho_{ij}(r)$ functions, namely ϱ_{CuCu}, ϱ_{CuCl} and ϱ_{ClCl}.

Equations (1) and (2) apply to liquids as well as to polycrystalline samples. Moreover, with neutron radiation, the values of b_i can be changed by varying the isotope composition of the chemical species i, and therefore one can, in principle, solve n observed CDSC's of the type in equation (1) for n unknown partial structure factors S_{ij}. This is the basis for the 'isotopic substitution technique' used by PM on liquid CuCl. After the S_{ij}'s have been obtained, a straightforward Fourier sine inversion of equation (2) yields ϱ_{ij} directly. Alternatively, if one has access to $m(\geq 1)$ CDSC patterns, one may model-fit $n(\geq 1)\varrho_{ij}$ curves, using a least-squares best approximation criterion. The confidence in the solution increases with an increase in m (for a given n). In this work, the second approach has been taken for reasons described below.

From equation (3), one obtains

$$G^E(r)=\frac{2}{\pi}\int_0^\infty F(\kappa)\sin \kappa r\mathrm{d}\kappa\,, \tag{5}$$

where the superscript E indicates the experimental origin of the structure function so obtained. From model curves for ϱ_{CuCu}, ϱ_{CuCl} and ϱ_{ClCl}, one finds a model structure function $G^M(r)$ *via* equation (4), which could be compared with $G^E(r)$ were it not for the fact that $F(\kappa)$ is only known up to κ_{max}, rather than infinity. The so called termination error on $G^E(r)$ that ensues has been discussed by Kaplow (1974). He states that one way of dealing with the problem is by fitting $G(r)$ to the known ϱ_0 for r less than nearest-neighbor distances. For a polyatomic solid, interference of the several $\varrho_{ij}(r)$ at small r, required the alternative approach to the termination error described below.

Terminating the integral in equation (5) at κ_m gives rise to a 'terminated experimental structure function'

$$G_t^E(r)=\int_0^{\kappa_m} F(\kappa)\sin \kappa r\mathrm{d}\kappa\,. \tag{6}$$

It is shown in Appendix *A* that $G(r)$ and $G_t(r)$ are related by an integral equation

$$G_t(r)=\int_0^\infty G(\xi)[u_t(\xi-r)-u_t(\xi+r)]\mathrm{d}\xi\,, \tag{7a}$$

with

$$u_t(x)=\frac{\sin \kappa_m x}{\pi x}. \qquad (7b)$$

In view of the δ-function-like character of $u_t(x)$, one may replace the upper limit in equation (7*a*) by $\xi_m \gg r$ and still obtain equality to any desired degree of accuracy by choosing ξ_m sufficiently large.

The model structure function $G^M(r)$ can be generated numerically up to large values of r and then artifically terminated using equation (7*a*) to obtain a 'terminated model structure function' $G_t^M(r)$. It is at this level that experiment and model are compared, and the parameters of the model are adjusted.

It should be noted that κ_m limits the resolution obtainable in $G(r)$, even when the instrumental resolution is perfect. Indeed, if $G^E(\xi)$ were a single δ function centered about $\xi=r_0$, the actual function found after Fourier transformation of the data would be

$$G_t^E(r)\simeq\int_0^\infty \delta(\xi-r_0)\frac{\sin \kappa_m(\xi-r)}{\pi(\xi-r)}\,\mathrm{d}\xi = \frac{\sin \kappa_m(r_0-r)}{\pi(r_0-r)}. \qquad (8)$$

From equation (8), the full width half maximum (FWHM) of G_t^E is $\sim 3{\cdot}8/\kappa_m$ (in units of r), limiting resolution to this value.

3. Experiment

(*a*) *The instrument*

The neutron cross sections were determined at the CP-5 reactor at Argonne National Laboratory. The data used in the Fourier analysis were taken with $\lambda=1{\cdot}05$ Å. The monochromator was a Ge crystal set for the 220 reflection. This reflection was chosen to improve instrumental resolution in the intermediate angle range, at the cost of incident intensity and some $\lambda/2$ contamination. Typical counting times at one 2θ position were 6 min for 10^6 monitor counts. The corresponding counting rates varied from 200 cpm (counts per min) in the background to 7000 cpm for the strongest peaks. All data points are averages of two runs at 10^6 monitor counts each. The half-wavelength incident intensity was determined to be $\sim 1\%$ of the full-wavelength incident intensity and was ignored during the analysis. The detector motion was restricted to $5°\leq 2\theta\leq 110°$ or, with $\kappa=4\pi \sin\theta/\lambda$, to $0{\cdot}5\leq\kappa\leq 10{\cdot}0$ Å^{-1}.

In addition to the main data, shorter runs were carried out at 5 and 80 K. For these experiments, the wavelength was 1·23 Å, which was obtained from the Ge 111 reflection. These data were used for integrated intensity analysis only. A purely elastic pattern at room temperature was also obtained by using a Ge 111 analyzer in the diffracted beam, and a detector fixed in the position for elastic scattering ($\lambda=1{\cdot}18$ Å). Additional energy analysis was obtained from a time-of-flight spectrum made at selected points in κ space using the TINTOF at CP-5.

(*b*) *Sample preparation*

Isotopically enriched samples of $^{63}Cu^{N}Cl$ and $^{65}Cu^{N}Cl$ (N=natural mixture)† and a commercially available $^{N}Cu^{N}Cl$ were purified and washed so as to obtain spectrographically clean samples of white color. The samples were enclosed in a thin-walled Pt cell under vacuum and heated to 366 °C in an aluminum-wall, radiant-heatfurnace. The scatteringvolume was defined by boron nitride plugs inside the cell. Typical samples were 1 inch in height, and $\frac{1}{2}$ inch in diameter, and the mass was ~ 5 g. For the low-temperature runs, the ^{63}CuCl was used, which was enclosed in a vanadium tube under atmospheric pressure. The elastic scattering measurements were performed on $^{N}Cu^{N}Cl$, also in a vanadium cell.

(*c*) *Measurements and corrections*

The three samples in the Pt cell were run twice at 366 °C and at room temperature. Empty-cell runs at both temperatures were corrected for absorption and subtracted. Fig. 1 shows a typical data set and the corresponding empty-cell run. A multiple-scattering correction was calculated after Blech & Averbach (1965), and a calculated (constant) incoherent component was also subtracted. The remaining intensity was scaled to absolute units by determining the scaling constant of the instrument *via* integrated intensities. Details of the data analysis are given by Schreurs (1974).

Fig. 2 shows the CDSC's thus obtained for the three samples at the two temperatures. The functions $s(\kappa^*)$ are plotted against $\kappa^*=\kappa a$ (a=lattice parameter) rather than κ for convenience in comparing runs at different temperatures. The large amount of diffuse scattering at 366 °C and the near disappearance of the reflections beyond $\kappa^*\simeq 30$ are most striking. The resolution of the instrument can be appreciated by referring to the Pt pattern in Fig. 1.

† Obtained from the Stable Isotope Division, Holifield National Laboratory, Oak Ridge, Tennessee.

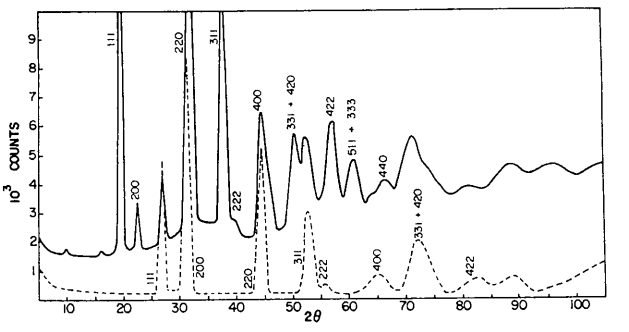

Fig. 1. Raw data from ^{63}CuCl (———) and empty platinum cell (-------) at 25 °C.

4. Integrated intensities

Integrated intensities were obtained from data in Fig. 2, with backgrounds estimated by linear extrapolation under peaks. At each temperature, data from the three samples were combined, which increased the number of independent reflections. Using the harmonic model, room-temperature data refined to $R_w=2{\cdot}2\%$ with 24 reflections, and $B_{Cu}=4{\cdot}3\pm0{\cdot}2$ Å^2 and $B_{Cl}=1{\cdot}9\pm0{\cdot}1$ Å^2 are in reasonable agreement with the results of SHH given in Table 1. Attempts to fit these data to the anharmonic model led to indentical values for R_w, B_{Cu} and B_{Cl} and an insignificantly small value for the anharmonic parameter β.

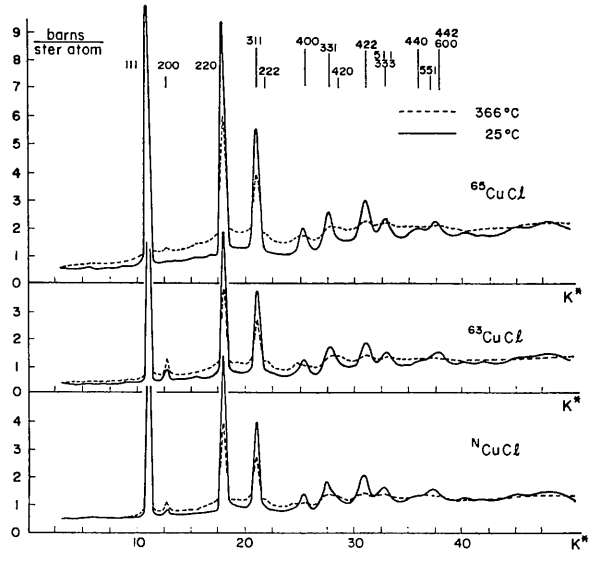

Fig. 2. Experimental values of $s(\kappa^*)$ *vs* κ^* $(=\kappa a)$ at 25 and 366°C for ^{65}CuCl, ^{63}CuCl and ^{N}CuCl.

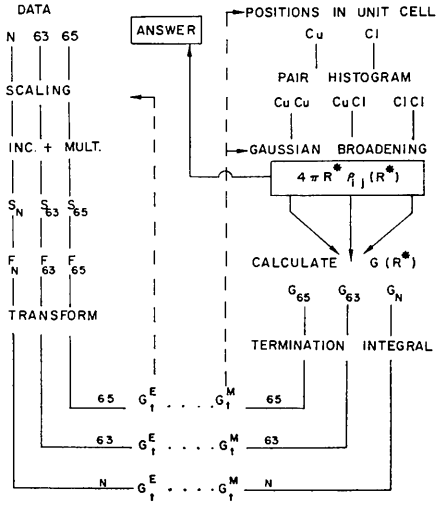

Fig. 3. Flow sheet for data reduction and model calculation in radial density analysis.

The 366°C data could also be fitted to a harmonic model, with $B_{Cu}=13{\cdot}0\pm1{\cdot}0$ and $B_{Cl}=4{\cdot}6\pm0{\cdot}4$ Å^2; however, difficulty in separating peaks from background is reflected in the large value of $R_w=7{\cdot}4\%$ for 21 reflections. At this high temperature, a larger degree of structural disorder is evidenced in the integrated intensities. Fitting to the anharmonic model reduces the agreement factor to $R_w=6{\cdot}4\%$ and assuming $\beta_{Cl}=0$ yields a value of $\beta_{Cu}=1{\cdot}2\pm0{\cdot}6\times10^{-2}$ erg Å^{-3}, which is in excellent agreement with the results of SHH. It is interesting to note that the large values of thermal parameters observed at elevated temperatures continue at lower temperatures. Data taken at 5 K on ^{63}Cu^{N}Cl were fitted with the harmonic model to yield the exceptionally large 'zero-point' values of $B_{Cu}=2{\cdot}6\pm0{\cdot}2$ and $B_{Cl}=1{\cdot}6\pm0{\cdot}1$ Å^2.

It is clear by reference to Fig. 2 that integrated intensities represent only a fraction of the structural information available in the powder diffraction pattern. In the remainder of the present paper, attention will be focused on alternative interpretations of these data, including the examination of diffuse scattering.

5. Radial density analysis

In § 2 it was noted that, with the three available neutron diffraction patterns, it is theoretically possible to obtain solutions for three 'partial structure factors' $S_{ij}(\kappa)$ [see equations (1) and (2)]. For solids, however, a special difficulty arises in attempting to establish the value of $s(\kappa)$ on the extremely steep slopes of Bragg peaks; slight errors in positioning will cause large errors in the value of $s(\kappa)$. For this reason, the second approach was chosen in this work, namely to fit the three data sets from a model, using least-squares techniques.

Fig. 3 shows a flow sheet of data handling and model building. These data are scaled to absolute cross sections (Fig. 2), and a constant, calculated value for the incoherent contribution and multiple scattering is subtracted. The $s(\kappa)$ curves so obtained are manipulated into $F(\kappa)$ curves [equation (4)] and then transformed to yield the terminated experimental structure functions $G_t^E(r)$, one for each isotopic composition.

The model building starts from the position of the atoms in the unit cell. For a given origin (Cu or Cl), the number of pairs of a given distance (in a single crystal) are counted and a 'pair histogram' is built. The equivalent number density of such a pair histogram $\varrho_{ij}(r)$ consists of a number of δ functions of different strengths c_{ij}^m,

$$4\pi r^2\varrho_{ij}(r)=\sum_m c_{ij}^m\delta(r-r_m)\,,\quad i,j=\mathrm{Cu,Cl}\,, \qquad (9)$$

where the sum is over all possible single-crystal distances between i and j atoms.

As a result of thermal vibrations, the density func-

tion actually contains a series of peaks of finite widths, and one writes

$$4\pi r^2 \varrho_{ij}(r) = \sum_m c_{ij}^m B_m(r - r_m) . \quad (10)$$

For the functions B_m, Gaussian curves were chosen. Following Kaplow (1974),

$$4\pi r \varrho_{ij}(r) = \sum_m c_{ij}^m \frac{\exp[-(r-r_m)^2/2(\sigma_{ij}^m)^2]}{r_m \sigma_{ij}^m \sqrt{2\pi}} . \quad (11)$$

In general, one σ_{ij}^m width parameter exists for each interatomic distance, but these parameters should obviously be related to the thermal vibration of the system. For monoatomic cubic crystals, the mean square vibrational amplitude is $\langle u^2 \rangle = 3\langle u_s^2 \rangle = 3B/(8\pi^2)$, where u_s is the vibrational amplitude projected in the diffraction direction. For such a crystal, the width parameter associated with the uncorrelated vibrations of distant atom pairs is $\sigma^\infty = 2\langle u_s^2 \rangle^{1/2}$. To account for coupling between neighboring atoms, Kaplow introduces the Walker–Keating coupling factors γ^m defined by

$$(\sigma^m)^2 = \gamma^m (\sigma^\infty)^2 \quad (12)$$

and

$$\lim_{m \to \infty} \gamma^m = 1 . \quad (13)$$

These concepts are readily extended to the binary CuCl system as follows:

$$(\sigma_{ij}^\infty)^2 = (B_i + B_j)/(8\pi^2) , \quad (14)$$

$$(\sigma_{ij}^m)^2 = \gamma_{ij}^m (\sigma_{ij}^\infty)^2 , \quad (15)$$

$$\lim_{m \to \infty} \gamma_{ij}^m = 1 , \quad i,j; \text{ Cu, Cl} . \quad (16)$$

Once the $4\pi r \varrho_{ij}(r)$ model curves are obtained, $G^M(r)$ is calculated from equation (4); the superscript M indicates the model nature of the function. To compare the model with experimental curves, equation (7) is used to produce a terminated model structure function $G_t^M(r)$, one for each isotopic composition. At this point, Powell's (1965) algorithm is used to minimize the sum of the squared differences between G_t^M and G_t^E, and the parameters are adjusted until a specified accuracy is obtained, or until failure to converge is detected.

A typical end product of such a procedure for the harmonic model is shown in Fig. 4, in which $G_t^M(R^*)$ and $G_t^E(R^*)$ *vs* $R^*(\equiv r/a)$ are plotted for room temperature ^{N}Cu^{N}Cl data. Successful treatment of termination errors is evidenced by the equally satisfactory fits at low and high R^*. The results of the fit may also be displayed as plots of $4\pi R^* \varrho_{ij}$, as shown in Figs. 5 and 6 for room temperature and 366 °C data, respectively. In both figures, the remarkable difference between ϱ_{ClCl} and ϱ_{CuCu} is displayed. The parameter values resulting from this fitting procedure are listed in Table 2. It is seen that B_{Cu} from radial density analysis is larger than that determined by the analysis of integrated intensities by a factor of two at both temperatures. A possible origin of this discrepancy as a consequence of instrument resolution is developed in Appendix *B*. The coupling factors used in the fits are also listed in Table 2. Particularly noteworthy is the small value of γ_{CuCl}^1, indicative of strong correlation in first-neighbor Cu–Cl distances.

An interesting comparison may be made between the present results at 366 °C and the liquid structure studied by PM, as shown in Fig. 7. The dotted curves represent the liquid CuCl at 440 °C, whereas the full curves are for the crystalline γ-phase at 366 °C. In Fig. 7, the results are presented as partial radial distribution

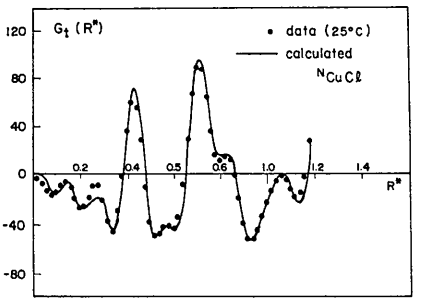

Fig. 4. Comparison of $G_t^M(R^*)$ (———) and $G_t^E(R^*)$ (· · · · · ·) *vs* R^* $(=r/a)$ for the ^{N}CuCl at 25 °C.

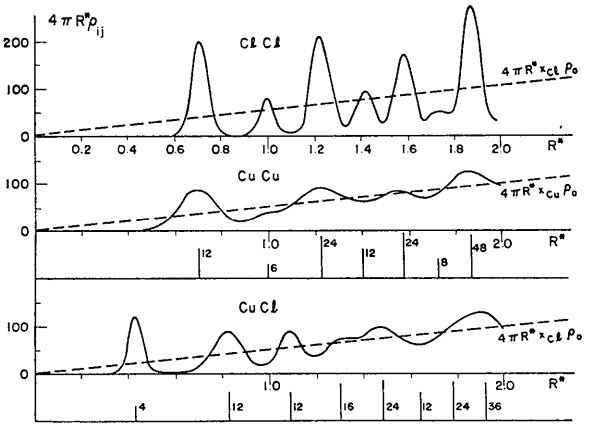

Fig. 5. Partial radial density functions for γ-CuCl at 25 °C.

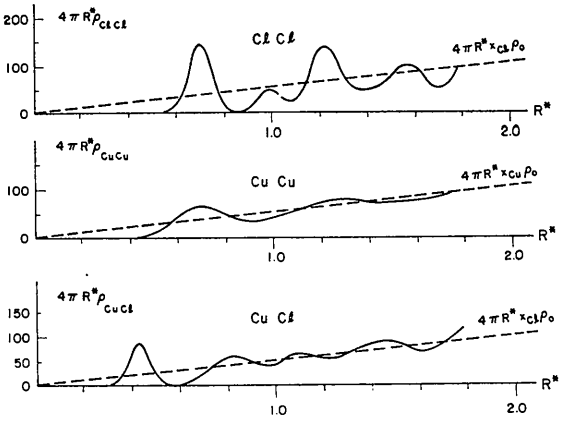

Fig. 6. Partial radial density functions for γ-CuCl at 366 °C.

functions $g_{ij}(r)=\varrho_{ij}(r)/x_j\varrho_0$. The Cl–Cl distribution in the solid state is typical for a crystalline structure (Fig. 7*c*). A striking resemblance is noted between the distribution functions of Cu–Cu at 366 °C and Cl–Cl in the liquid state (Fig. 7*b*). The total lack of correlation exhibited in the Cu–Cu distribution for the liquid state has been discussed by PM. It should be noted that the oscillations near the origin in the curves for the liquid are due to termination error, an effect taken into account in the present study of γ-CuCl.

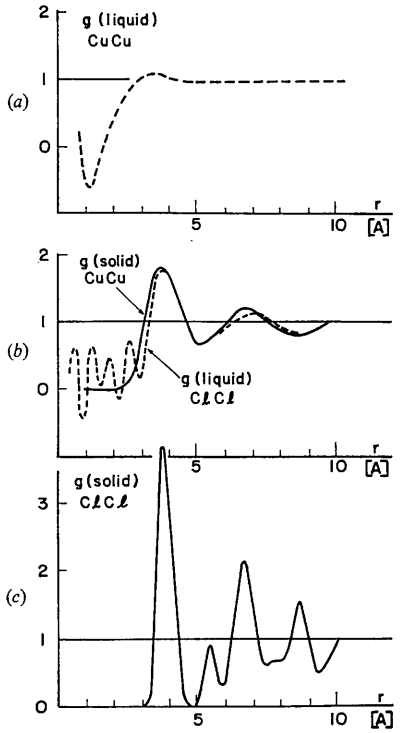

Fig. 7. Partial radial distribution functions, *g*, for (*a*) CuCu found in liquid CuCl at 440 °C (-------), (Page & Mika, 1971); (*b*) CuCu and (*c*) ClCl found in solid γ-CuCl at 366 °C (———), this work.

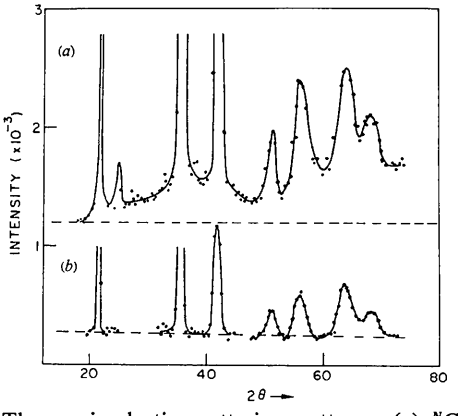

Fig. 8. Three-axis elastic scattering patterns, (*a*) $^{N}Cu^{N}Cl$ at 25 °C and (*b*) Si powder at 25 °C.

Table 2. *Values of the parameters of the radial density analysis (harmonic model)*

Temperature	25 °C	366 °C	
B_{Cu}	10·5 ±1·0 Å²	23·6 ±3·5 Å²	
B_{Cl}	1·9 ±0·5	4·9±1·5	
Coupling factors ($\gamma^l_{CuCu}=\gamma^l_{ClCl}$)			
			Shell number
γ^1 (CuCl)	0·16±0·01	0·14±0·01	1
γ^1 (CuCu)	0·74±0·1	0·56±0·1	2
γ^2 (CuCl)	0·87±0·2	0·73±0·3	3
γ^2 (CuCu)	0·72±0·1	0·60±0·1	4
γ^3 (CuCl)	0·52±0·4	0·45±0·4	5
γ^3 (CuCu)	0·79±0·2	0·87±0·3	6
γ^4 (CuCl)	1·0	0·76±0·4	7
γ^4 (CuCu)	1·0	1·25±0·4	8
γ^5 (CuCl)	1·0	0·68±0·4	9
γ^5 (CuCu)	1·0	1·05±0·4	10
γ^6 (CuCl)	1·0	0·63±0·4	11
γ^6 (CuCu)	1·0	1·3 ±0·4	12

The results of Fig. 7 indicate that in both the solid and liquid states the Cu–Cu distribution is broader and flatter than the Cl–Cl distribution. Although the effects of errors inherent in the technique (*e.g.* termination and instrumental resolution) may affect the absolute values of the parameters, the qualitative distinction between the two distributions is clear. It should be emphasized that the liquid-state results are solutions of the isotopic equations, whereas the present study relies on model fitting.

6. The nature of the diffuse scattering

Although indistinguishable with regard to integrated intensities, the anharmonic and disordered models would give rise to different types of diffuse scattering. For the anharmonic model, all diffuse scattering should be inelastic, arising from the dynamic motions of the atoms. On the other hand, a statistically disordered structure would exhibit an elastic component of the diffuse scattering as a result of statically displaced copper ions. It might be expected that, if the anharmonic model were correct, the larger values of B_{Cu} obtained from the radial density analysis would be due to the inclusion of the inelastic diffuse scattering in this analysis.

To check the nature of the diffuse scattering, a purely elastic three-axis run was performed on the $^{N}Cu^{N}Cl$ sample ($\lambda=1{\cdot}18$ Å). Fig. 8(*a*) shows the scattering obtained from such a sample enclosed in vanadium at room temperature. A silicon standard (also in vanadium) is shown in Fig. 8(*b*). Using a similar sample, a time-off-flight energy analysis was made at selected points of κ space. This spectrum revealed that the first inelastic maximum of the scattering law $S(\kappa,\omega)$ lies well outside the 2·25 meV resolution of the analyzing crystal in the three-axis experiment. Throughout the κ-range of investigation, the first maximum in the ω direction occurred between 4 and 4·5 meV. As can be seen from Fig. 8(*a*), a significant portion of the diffuse scattering

is still present in the elastic pattern. The silicon pattern (similar structure, cross sections and lattice parameter) indicates that no other instrumental effects cause the background increase in the CuCl and, incidentally, that an angle-independent multiple-scattering correction is quite reasonable.

From a comparison of the three-axis run with the two-axis runs, it is estimated that 50 to 70% of the diffuse scattering is elastic ($\pm 2{\cdot}25$ meV), indicating that some type of displacement disorder exists in the system. A statistical distribution of the Cu atoms over the (x,x,x) equipoint, however, will not give rise to this κ-dependent diffuse background, and more complex models, probably with correlated displacements, must be considered.

Having established that the diffuse scattering is primarily elastic, it remains to explain why radial density analysis gives rise to higher B values than the integrated intensity analysis. It is shown in Appendix B that the resolution of the instrument introduces an error in the widths of the radial density peaks. The nature of the error is such that peaks farther away from the origin are broadened more than peaks closer to the origin. Setting $\gamma_{ij}^m = 1$ from a particular value m_0 onward, will fix the 'temperature factor' (rather arbitrarily), absorbing the resolution error in σ^∞. From the results in Appendix B, it appears that the widths of the peaks at the reduced radial distance of $\sim 1{\cdot}5$ lattice parameters are 50 to 100% broadened. This would cause least-squares B factors to be too large by a factor of two to three, if the coupling factors are set equal to 1·0 at this distance and beyond.

7. Conclusions

From integrated intensity analysis, it appears that γ-CuCl can be described as zincblende type, with structural disorder of the copper ions describable in terms of an anharmonic or statistical-disorder model. The diffuse scattering was found to be a mixture of elastic and inelastic scattering. At room temperature, ~50 to 70% of the scattering is elastic. Since an anharmonic zincblende structure does not explain this scattering, a model of 'correlated' displacements that will give the observed distribution of elastic coherent diffuse scattering needs to be developed.

The radial density analysis, unfortunately, is strongly affected by instrumental resolution and can only provide qualitative information. In general terms, the Cu–Cu distribution is much broader and less well defined than the Cl–Cl distribution. Since both of these curves are based on the same model histogram, the broad Cu–Cu distribution is qualitatively viewed as a 'smearing' of the sharp Cl–Cl distribution due to correlated disorder of the Cu ions in the Cl tetrahedra. This concept may be extended to describe the liquid CuCl results of PM. The Cl–Cl distribution in the liquid may be thought of as Cl tetrahedra, with a dynamically varying distribution of bond lengths and angles, which is analogous to the supposed structures o amorphous Ge and Si. In these Cl tetrahedra, structurally disordered Cu ions would produce an additional 'smearing' of the liquid Cl–Cl distribution to form the nearly correlation-free distribution measured for Cu–Cu by PM and presented in Fig. 7(*a*).

The situation in radial density analysis is rather unsatisfactory. Most errors (*e.g.* termination and scale factor) primarily affect the region of r space near the origin and the first peaks. The instrumental resolution error takes over where the other errors disappear. It is apparent from the results in Appendix B that resolution problems will have significant effects on the details of the radial density curves in both liquid and solid state investigations.

The authors would like to acknowledge the assistance of Drs K. Sköld and C. Pelazzari for their experimental and analytical assistance in the time-of-flight experiment. Thanks are also due Dr LeRoy Heaton for the initial efforts in isotopic sample characterization and Dr J. Faber for his helpful discussions regarding the integrated intensity analysis. One of us (J.S.) expresses his appreciation to the Argonne Center for Educational Affairs and the Materials Science Division of Argonne National Laboratory for support under a thesis parts program.

APPENDIX *A*

Correction for termination error

The following theorem is proven in most textbooks on Fourier analysis or distribution theory: if $\varphi(x)$ is continuously differentiable on $-\infty < x < +\infty$ and $\varphi(x) \equiv 0$ for $|x| > R$ then

$$\lim_{k\to\infty} \int_{-\infty}^{+\infty} \frac{\sin kx}{\pi x} \varphi(x)\mathrm{d}x = \varphi(0)\,. \qquad (A1)$$

This theorem is equivalent to the statement

$$\lim_{k\to\infty} \frac{\sin kx}{\pi x} = \delta(x) \text{ on } D^1, \qquad (A2)$$

where it is understood that D^1 is the class of functions $\varphi(x)$ defined in the theorem. The restriction of the discussion to D^1 is sufficient, not necessary; the radial density functions of diffraction theory belong to D^1.

If one now has a function $\varphi(x)$ in D^1, then

$$\psi(k) = \int_0^\infty \varphi(x) \sin kx\mathrm{d}x \quad -\infty < k < +\infty \qquad (A3)$$

exists and is called the Fourier sine transform of $\varphi(x)$. Consider now the 'terminated Fourier back-transform'

$$F_m(\xi) = \frac{2}{\pi} \int_0^{k_m} \psi(k) \sin k\xi\mathrm{d}k$$

$$= \frac{2}{\pi} \int_0^\infty \psi(k)[H(k+k_m) - H(k-k_m)] \sin k\xi\mathrm{d}k. \qquad (A4)$$

Substituting (*A*3) into (*A*4), performing the k integration first and using the relation $\sin kx \sin k\xi = [\cos k(\xi - x) - \cos k(\xi + x)]/2$ produces two integrals of the form

$$\frac{1}{\pi}\int_{-\infty}^{+\infty}[H(k+k_m)-H(k-k_m)]\cos k\xi \mathrm{d}k = \frac{\sin k_m\xi}{\pi\xi} = u_m(\xi)\,. \quad (A5)$$

The Heaviside distribution $H(\alpha)$ is defined by

$$\int_{-\infty}^{+\infty} H(\alpha)\varphi(\alpha)\mathrm{d}\alpha = \int_0^{\infty}\varphi(\alpha)\mathrm{d}\alpha \text{ for } \varphi\in D^1.$$

One finds

$$F_m(\xi) = \int_0^{\infty}\varphi(x)[u_m(|x-\xi|)-u_m(|x+\xi|)]\mathrm{d}x\,, \quad (A6)$$

with $u_m(\xi)$ defined by (*A*5). From (*A*2) it follows immediately that

$$\lim_{k_m\to\infty} F_m(\xi) = \varphi(\xi)\,. \quad (A7)$$

The treatment closely follows a derivation given by Warren (1969). The effect of a space averaging convergence factor is discussed by Schreurs (1974).

APPENDIX *B*

The effect of instrumental resolution on radial density analysis

To demonstrate the effect of instrumental resolution on radial density analysis, a comparison was made between two numerically synthesized radial density functions (RDF) for the same hypothetical sample. In the computation of the first RDF, the instrumental resolution was assumed to be perfect, and the CDSC 'measured' up to $\kappa_m^* = 63$. Although still subject to termination error, this RDF will be referred to as the 'ideal' RDF, $G_{ti}(R^*)$. The same CDSC curve was then convoluted with a Gaussian resolution function and the resultant cross sections were used to calculate the second RDF which exhibits the effects of termination and instrumental resolution, and will be identified as the 'measured' RDF, $G_{tm}(R^*)$.

The CDCS per steradian per unit cell, $s(\kappa^*)$ for an ideal polycrystalline sample can be expressed in terms of the structure factors (c_i) for each reflection ($i = h,k,l$) as follows:

$$s(\kappa^*) = (2\pi)^3 \sum_i c_i\delta(\kappa^* - \kappa_i^*)/(4\pi\kappa^{*2})\,. \quad (B1)$$

Using equations (6) and (4) in the text the RDF $G_{ti}(R^*)$ may then be written:

$$G_{ti}(R^*) = 4\pi\sum_i^{\kappa_m^*}\left(c_i\frac{\sin\kappa_i^*R^*}{\kappa_i^*}\right) - 2D_m(R^*)/\pi\,, \quad (B2)$$

where

$$D_m(R^*) = \frac{\sin\kappa_m^*R^*}{R^{*2}} - \frac{\kappa_m^*}{R^*}\cos\kappa_m^*R^*.$$

To simulate the measurement of $s(\kappa^*)$ on a conventional two-axis diffractometer, 'observed' data, $s_0(\kappa^*)$, was calculated by convoluting $s(\kappa^*)$ with the resolution function $g(\kappa^*,\kappa')$:

$$s_o(\kappa^*) = \int s(\kappa')g_{\kappa^*}(\kappa^* - \kappa')\mathrm{d}\kappa', \quad (B3)$$

where

$$g_{\kappa^*}(\zeta) = \exp[-\zeta^2/(2\sigma_{\kappa^*}^2)]/(\sigma_{\kappa^*}\sqrt{2\pi})\,.$$

The subscript κ^* indicates that the resolution function depends parametrically on the point of observation. Substituting (*B*1) into (*B*3), and using the fact that σ_{κ^*} varies slowly with κ^*:

$$s_o(\kappa^*) = 2^{1/2}\pi^{3/2}\sum_i c_i \exp[-(\kappa^* - \kappa_i^*)^2/(2\sigma_i^2)]/(\sigma_i\kappa_i^{*2})\,, \quad (B4)$$

where σ_i^2 is the variance of the Gaussian resolution function at κ^*.This 'observed' structure function may then be used with (6) and (4) to obtain the measured RDF, $G_{tm}(R^*)$. The analytical expression obtained by reasonable approximation for the present case, $\sigma_i \ll \kappa_i^*$, is:

$$G_{tm}(R^*) = \sum_i \frac{4\pi c_i}{\kappa_i^{*2}}(\kappa_i^*\sin\kappa_i^*R^* + \sigma_i^2R^*\cos\kappa^*R^*) \times \exp(-R^{*2}\sigma_i^2/2) - 2D_m/\pi\,. \quad (B5)$$

In the limit, when all σ_i approach zero, G_{tm} approaches G_{ti} as required.

Fig. 9 shows 'ideal' and 'measured' RDF's for the same $s(\kappa^*)$. 33 non-zero structure factors were computed for a diamond-type crystal with $b^2 = 1$ barn and a temperature factor $B = 0{\cdot}5$ Å^2. For a lattice parameter of $a = 5{\cdot}416$ Å this would correspond to a cut-off at $\kappa = 11{\cdot}6$ Å^{-1}. The resolution function $g_{\kappa^*}(\zeta)$ was typical of that for the instrument described in the main text.

Common practice in radial density analysis of scattering from polycrystalline specimens is to fit the $G_t(R^*)$ curves to Gaussians. The widths of the Gaussians are then related to the vibrational characteristics of the system [equation (9)–(16)]. Writing w_i^* for the HWHM of the ith Gaussian in the representation of G_t, one has

$$w_i^* \cong (1{\cdot}386\gamma_iB)^{1/2}/(2\pi a) \quad (B6)$$

where the γ_i are the coupling constants. When this analysis is applied to the RDF's of Fig. 9, the 'ideal' G_{ti} consists of peaks of virtually constant widths ($2w_i^* \simeq 0{\cdot}07$ for all i) in good agreement with the resolution limit expected from termination error ($2w_{\min}^* \simeq 0{\cdot}06$). These results correspond to $\gamma_i = 1{\cdot}0$ for all i, and $B =$

1·024 Å^2. This factor of two increase in B for the ideal RDF over the input value of $B=0{\cdot}5$ Å^2 is due to termination error and may be eliminated as described in the text.

The effect of instrumental resolution on the RDF is exhibited in the solid curve for $G_{tm}(R^*)$ in Fig. 9 which exhibits a series of peaks whose widths increase with R^*. Since B is taken constant in ($B6$), the increase in w_i^* with R^* has to be absorbed by the γ_i. The absolute values of these parameters will depend on the choice of R_c^*, the point beyond which all γ_i's are set equal to unity in the analysis. This same choice will also rather arbitrarily set the value of B, which will be heavily weighted by the broadened peaks beyond R_c^* if a least-squares criterion is used. From G_{tm} in Fig. 9, B values may be obtained which are two or three times as high as the one obtained from G_{ti}.

Unfortunately, correcting for the resolution error is much more difficult than demonstrating the need for such a correction. The simplified case, at the basis of the present exposition, is of little interest in most radial density analyses. Where this type of analysis would be most useful, *e.g.* in the study of liquids and amorphous solids, $s(\kappa^*)$ can no longer be represented by ($B1$), *i.e.* the observed $\kappa^{*2}s_o(\kappa^*)$ is no longer simply a sum of Gaussian functions.

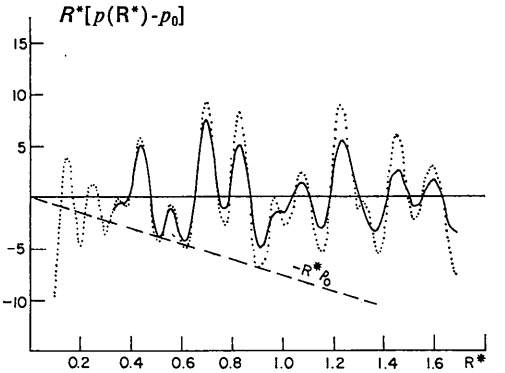

Fig. 9. The effect of instrumental resolution on the radial density for δ-function-like instrumental resolution, $G_{ti}(R^*)$, (·····), and for a typical neutron spectrometer resolution function, $G_{tm}(R^*)$, (———). Both curves are uncorrected for termination error.

References

BLECH, I. A. & AVERBACH, B. L. (1965). *Phys. Rev. A*, **137**, 1113–1116.

HELMOHOLZ, L. (1935). *J. Chem. Phys.* **3**, 740–747.

HOSHINO, S. (1952). *J. Phys. Soc. Japan*, **7**, 560–564.

HOSHINO, S. (1954). *J. Phys. Soc. Japan*, **9**, 295.

HOSHINO, S. (1955). *J. Phys. Soc. Japan*, **10**, 197–200.

HOSHINO, S. (1957). *J. Phys. Soc. Japan*, **12**, 315–326.

KAPLOW, R. (1974). *X-ray Diffraction*, by L. V. AZAROFF, R. KAPLOW, N. KATO, R. J. WEISS, A. J. C. WILSON & R. A. YOUNG, Chap. 2. pp. 79–140. New York: McGraw-Hill.

KEATING, D. T. (1963). *J. Appl. Phys.* **34**, 923–925.

MIYAKE, S. & HOSHINO, S. (1958). *Rev. Mod. Phys.* **30**, 172–174.

MIYAKE, S., HOSHINO, S. & TAKENAKA, T. (1952). *J. Phys. Soc. Japan*, **7**, 19–24.

PAGE, D. I. & MIKA, K. (1971). *J. Phys. Chem.* **4**, 3034–3044.

POWELL, M. J. D. (1965). *Comput. J.* **7**, 303–307.

SAKATA, M., HOSHINO, S. & HARADA, J. (1974). *Acta Cryst.* A**30**, 655–661.

SCHREURS, J. (1974). Ph. D. Thesis, Northwestern Univ.

STROCK, L. (1936). *Z. Phys. Chem.* B**31**, 132–136.

VINEYARD, G. H. (1958). *Liquid Metals and Solidification*, pp. 35–36. Cleveland: American Society for Metals.

WARREN, B. E. (1969). In *X-Ray Diffraction*, p. 127. Reading, Mass.: Addison-Wesley.